CHEMISTRY
AN ASIAN JOURNAL

DOI: 10.1002/asia.200700152

A Two-Dimensional Coordination Compound as a Zinc Ion Selective Luminescent Probe for Biological Applications

Koushik Dhara,[a] Santanu Karan,[b] Jagnyeswar Ratha,[c] Partha Roy,[a] Goutam Chandra,[d] Mario Manassero,[e] Biswanath Mallik,[b] and Pradyot Banerjee*[a]

Abstract: A 2D coordination compound $\{[Cu_2(HL)(N_3)]\cdot ClO_4\}_\infty$ (**1**; H_3L = 2,6-bis(hydroxyethyliminoethyl)-4-methyl phenol) was synthesized and characterized by single-crystal X-ray diffraction to be a polymer in the crystalline state. Each $[Cu_2(HL)(N_3)]^+$ species is connected to its adjacent unit by a bridging alkoxide oxygen atom of the ligand to form a helical propagation along the crystallographic *a* axis. The adjacent helical frameworks are connected by a ligand alcoholic oxygen atom along the crystallographic *b* axis to produce pleated 2D sheets. In solution, **1** dissociates into $[Cu_2(HL)_2(H_3L)]\cdot 2H_2O$ (**2**); the monomer displays high selectivity for Zn^{2+} and can be used in HEPES buffer (pH 7.4) as a zinc ion selective luminescent probe for biological application. The system shows a nearly 19-fold Zn^{2+}-selective chelation-enhanced fluorescence response in the working buffer. Application of **2** to cultured living cells (B16F10 mouse melanoma and A375 human melanoma) and rat hippocampal slices was also studied by fluorescence microscopy.

Keywords: biosensors · copper · fluorescent probes · luminescence · zinc sensors

Introduction

There is much current interest in elucidating the role of bivalent zinc in neurobiology.[1] Although Zn^{2+} homeostasis is tightly regulated by a number of homologous Zn^{2+} transporter proteins (ZnTs)[2] and metallothioneins,[3] pools of loosely bound or "free" Zn^{2+} occur in the mossy fiber terminals of the hippocampus, the center of learning and memory in the brain.[4] Zinc concentrations of about 0.3 mM are achieved in vesicles in the presynaptic terminals of the cells. It is the second-most-abundant metal ion in the human body: the total concentration in serum is in the micromolar range.[5] Zinc-containing enzymes (e.g., carbonic anhydrase) are well-known and play critical roles in maintaining the key structural features of zinc transcription proteins (e.g., zinc finger proteins).[1b,6] Apart from that, high concentrations of free or loosely bound Zn^{2+} are present in the pancreas[7] and spermatozoa.[8] A number of biological functions are regulated by labile Zn^{2+}, such as suppression of apoptosis,[9] contribution to neuronal injury in certain critical states,[10] epilepsy,[11] and induction of the formation of β-amyloids[12] related to the etiology of Alzheimer's disease. Although many reports describe the significance of chelatable Zn^{2+} in biological systems, its mechanisms of action are less understood[13] than those of other cations, such as Ca^{2+},

[a] K. Dhara, P. Roy, Dr. P. Banerjee
Department of Inorganic Chemistry
Indian Association for the Cultivation of Science
Jadavpur, Kolkata-700032 (India)
Fax: (+91) 33-2473-2805
E-mail: icpb@mahendra.iacs.res.in

[b] S. Karan, Dr. B. Mallik
Department of Spectroscopy
Indian Association for the Cultivation of Science
Jadavpur, Kolkata-700032 (India)

[c] J. Ratha
Cellular Biochemistry Division
Indian Institute of Chemical Biology
Jadavpur, Kolkata-700032, India

[d] G. Chandra
Division of Clinical and Experimental Neurosciences
Indian Institute of Chemical Biology
Jadavpur, Kolkata-700032 (India)

[e] Dr. M. Manassero
Dipartimento di Chimica Strutturale e Stereochimica
Inorganica dell'Università di Milano
Via G. Venezian 21
20133 Milano (Italy)

Supporting information for this article is available on the WWW under http://www.chemasianj.org or from the author.

 © 2007 Wiley-VCH Verlag GmbH & Co. KGaA, Weinheim

Na^+, and K^+. A continued effort to detect chelatable or labile Zn^{2+} in biological systems is being made.[14]

To elucidate the role of Zn^{2+} in such events, detection methods that exhibit selectivity and sensitivity toward Zn^{2+} and that are also suitable for use in biological fluids are required.[14,15] Fluorescent zinc chemosensors have been developed for imaging biological Zn^{2+}.[16] These probes include aryl sulfonamide derivatives of 8-aminoquinoline, such as 6-methoxy-(8-*p*-toluenesulfonamido)quinoline (TSQ),[17] as well as Zinquin,[18] Zinbo-5,[19] the Zinpyr (ZP) family,[20] and the ZnAF molecules.[21] Besides these small-molecule sensors, synthetic peptides can also signal zinc by fluorescence enhancement.[22] A variety of Zn^{2+}-selective sensor molecules[23] were also reported based on f- or d–f (mixed)-block elements. These are discrete molecules or multidimensional porous coordination polymers.[23c,d] To our knowledge, there are no reports of any study of zinc ion selective luminescent sensing property in a 3d-metal-based coordination compound. Herein we report a 2D coordination compound, $\{[Cu_2(HL)(N_3)]\cdot ClO_4\}_\infty$ (**1**; H_3L = 2,6-bis(hydroxyethyliminoethyl)-4-methylphenol), that dissociates in water to give $[Cu_2(HL)_2(H_3L)]\cdot 2H_2O$ (**2**), which acts as a selective luminescent probe for zinc ion. The investigation into the luminescent property in HEPES (4-(2-hydroxyethyl)-1-piperazineethanesulfonic acid) buffer (pH 7.4) showed that the emission intensity of **1** increased significantly ($\approx$19-fold) upon addition of Zn^{2+}, whereas the introduction of other metal ions caused the intensity to be either unchanged or weakened. These results imply that **1** can be used to monitor or recognize Zn^{2+} and, therefore, be considered as a selective luminescent probe. By incubating cultured living cells or rat hippocampal slices with **1**, both intracellular and free Zn^{2+} concentration in hippocampal slices can be monitored.

Abstract in Bengali:

একটি দ্বিমাত্রিক জটিল যৌগ $\{[Cu_2(HL)(N_3)].ClO_4\}_\infty$ (**1**) (H_3L=2,6-bis(hydroxyethyliminoethyl)-4-methyl phenol) সংশ্লেষ করা হয়েছে এবং এর একক ক্রিস্টালের X-ray diffraction বিশ্লেষণ দ্বারা প্রমাণিত হয়েছে যে কঠিন অবস্থায় যৌগটি একটি polymer। প্রত্যেক $[Cu_2(HL)(N_3)]^+$ একক তার নিকটবর্তী এককের সঙ্গে alkoxide oxygen পরমাণু দ্বারা যুক্ত হয়ে আছে এবং এটি crystallographic *a*-অক্ষ বরাবর helix রূপে বিস্তার লাভ করেছে। আবার নিকটবর্তী helix খাঁচাগুলি নিজেদের মধ্যে alcoholic oxygen পরমাণু দ্বারা crystallographic *b*-অক্ষ বরাবর যোগাযোগ স্থাপন করেছে। সামগ্রিক ভাবে এটি একটি খন্ডিত দ্বিমাত্রিক sheet-এর রূপ ধারণ করেছে। দ্রবীভূত অবস্থায় যৌগ (**1**) টি ভেঙ্গে যায় এবং একটি নতুন যৌগ, $\{[Cu_2(HL)_2(H_3L)].2H_2O\}$, (**2**) তৈরি করে। এই নতুন যৌগটি অন্যান্য ধাতব আয়নের মধ্যে থেকে Zn^{2+} আয়নকে শনাক্ত করতে পারে এবং তাই এটিকে Zn-selective luminescent probe হিসাবে HEPES buffer-এ (pH 7.4) জীববিজ্ঞান সংক্রান্ত প্রয়োগে ব্যবহার করা যেতে পারে। এই প্রণালীটি ঐ buffer-এ প্রায় 19 গুণ chelation ঘটিত fluorescence প্রতিক্রিয়া দেখায়। যৌগ **2**-কে fluorescent অনুবীক্ষণ যন্ত্রের সাহায্যে জীবিত কোষ (B16F10 mouse melanoma এবং A375 human melanoma) এবং ইঁদুরের hippocampal slices-এর উপর প্রয়োগ সংক্রান্ত অনুধাবন করা হয়েছে।

Results and Discussion

Structure of Complex 1

Complex **1** was structurally characterized by X-ray crystallography. The data collection and refinement parameters are given in Table 1. Single-crystal X-ray analysis shows that the infinite 2D coordination framework is generated by the cross-linking of $\{[Cu_2(HL)(N_3)]\cdot ClO_4\}_\infty$ (**1**) chains into a sheet structure connected by the alcoholic oxygen atom (Figure 1). The asymmetric unit contains a dinuclear Cu^{2+} species $[Cu_2(HL)(N_3)]^+$, in which the Cu^{2+} atoms are bridged by the azide ion in an end-on fashion (Figure 2). One of the copper ions (Cu1) shows distorted square-planar geometry with two oxygen (O1, O2) and one nitrogen atom (N1) of the ligand and N3 of the azide ion. The other copper ion, Cu2, displays distorted square-pyramidal geometry with two nitrogen atoms (N2, N3) of the ligand (HL) and azide ion, respectively, and three oxygen atoms (O1, O2, O3); O2 and O3 are from the ligand of the other dinuclear unit. Selected bond lengths and angles are listed in Table 2. The long Cu2–O3 distance is 2.305(2) Å. Here each $[Cu_2(HL)(N_3)]^+$ species is connected to its adjacent unit by the bridging alkoxide oxygen atom (O2) of the ligand to form a helical propagation along the crystallographic *a* axis. The Cu–Cu distance in the asymmetric unit is 3.045(1) Å. The helical framework

Table 1. Crystallographic data for **1**.

	1
Formula	$C_{13}H_{16}ClCu_2N_5O_7$
M_r	516.83
Color	dark green
Crystal system	orthorhombic
Space group	*Pbca* (No. 61)
a [Å]	8.7996(6)
b [Å]	18.117(1)
c [Å]	21.617(2)
U [Å]	3446.2(5)
Z	8
F(000)	2080
D_c [g cm^{-3}]	1.992
T [K]	150
Crystal dimensions [mm]	0.15×0.20×0.22
$\mu(Mo_{K\alpha})$ [cm^{-1}]	26.82
Min. and max. transmission factors	0.902–1.000
Scan mode	ω
Frame width [°]	0.30
Time per frame [s]	20
No. of frames	2470
Detector–sample distance [cm]	4.00
θ range [°]	3–28
Reciprocal space explored	full sphere
No. of reflections (total, independent)	48947, 4173
R_{int}	0.0361
Final *R*2 and *wR*2 indices[a] (F^2, all reflections)	0.061, 0.082
Conventional *R*1 index ($I>2\sigma(I)$)	0.035
Reflections with $I>2\sigma(I)$	2915
No. of variables	265
Goodness of fit[b]	1.077

[a] $R2=[\Sigma(|F_o^2-kF_c^2|/\Sigma F_o^2]$, $wR2=[\Sigma w/(F_o^2-kF_c^2)^2/\Sigma w(F_o^2)^2]^{1/2}$. [b] $[\Sigma w\times(F_o^2-kF_c^2)^2/(N_o-N_v)]^{1/2}$, in which $w=4F_o^2/\sigma(F_o^2)^2$, $\sigma(F_o^2)=[\sigma^2(F_o^2)+(pF_o^2)^2]^{1/2}$, N_o is the number of observations, N_v is the number of variables, *p* is the ignorance factor 0.03.

 © 2007 Wiley-VCH Verlag GmbH & Co. KGaA, Weinheim

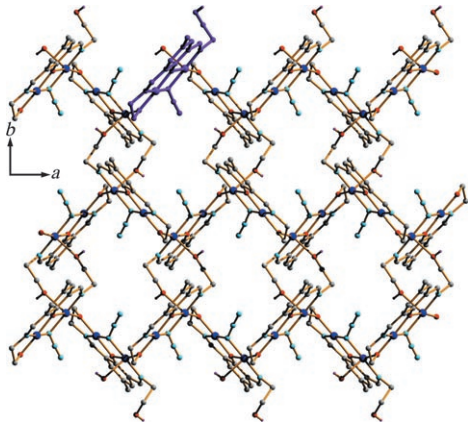

Figure 1. View of an infinite 2D coordination framework generated by the cross-linking of $\{[Cu_2(HL)(N_3)]\cdot ClO_4\}_\infty$ (**1**) chains into a sheet structure connected by the alcoholic oxygen atoms. H atoms (except H1) and ClO_4^- anions are omitted for clarity. ● = Cu, ● = O, ● = N, ● = C, ● = H.

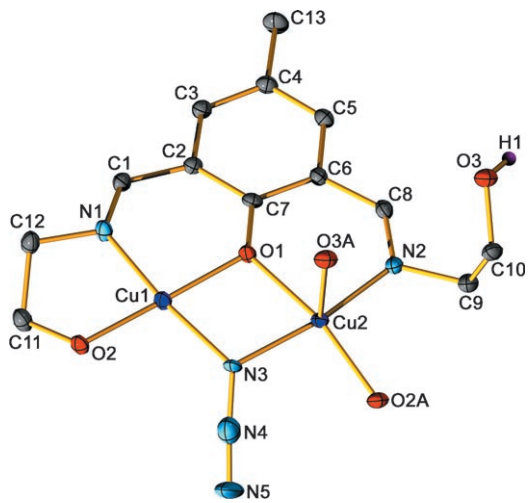

Figure 2. ORTEP drawing and atom numbering scheme for the dimeric unit of $\{[Cu_2(HL)(N_3)]\cdot ClO_4\}_\infty$ (**1**). H atoms (except H1) and ClO_4^- anions are omitted for clarity.

Table 2. Selected bond lengths (Å) and angles (°) for **1**.[a]

Cu1–N1	1.915(2)	Cu1–O1	1.950(2)
Cu1–N3	1.954(2)	Cu1–O2	1.912(2)
Cu1–N4	2.867(3)	Cu2–O1	1.987(2)
Cu2–N2	1.959(2)	Cu2–O2b	1.945(2)
Cu2–N3	1.994(2)	Cu2–O3c	2.306(2)
Cu2–N4	2.807(3)		
N1–Cu1–N3	172.75(10)	O3c–Cu2–N2	93.09(8)
N1–Cu1–N4	163.19(9)	N3–Cu2–N4	22.91(10)
N3–Cu1–N4	20.54(9)	O2b–Cu2–N3	93.74(9)
N2–Cu2–N3	169.45(9)	O3c–Cu2–N3	90.04(8)
N2–Cu2–N4	160.94(10)	O2b–Cu2–N4	73.40(8)
O2b–Cu2–N2	95.47(9)	O3c–Cu2–N4	104.17(8)
O2b–Cu2–O3c	101.72(7)		

[a] Symmetry codes: b = $^1/_2+x$, $-^1/_2-y$, $1-z$; c = $-x$, $-y$, $1-z$.

is built by Cu2–O1–Cu1–O2 repeating units, in which the angles Cu2–O1–Cu1 and Cu1–O2–Cu2 are 101.3(1) and 127.5(1)°, respectively. The adjacent helical frameworks are connected by the ligand alcoholic oxygen atom, O3, along the crystallographic *b* axis to give pleated 2D sheets (Figure 3). The interlayer separations are Cu1–Cu1 = 10.809(1), Cu2–Cu2 = 11.322(1), and Cu1–Cu2 = 9.219(1) Å. The section of the 2D sheet shown displays a decanuclear macrocycle of composition $Cu_{10}C_4O_{10}N_2$.

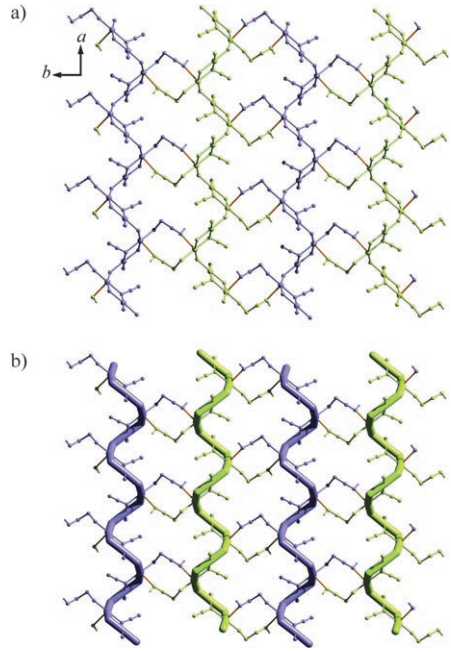

Figure 3. a) Infinite 2D coordination framework generated by the cross-linking of $\{[Cu_2(HL)(N_3)]\cdot ClO_4\}_\infty$ (**1**) helical chains into a sheet structure connected by the alcoholic oxygen atom of the ligand. b) Helical propagation along the crystallographic *a* axis to form pleated 2D sheets. C and H atoms (except H1) and ClO_4^- anions are omitted for clarity. The right- and left-handed helical structures are indicated by violet and green, respectively.

Fluorescence Properties and Metal-Ion-Competition Studies

The emission spectrum of **1** in 100 mM HEPES buffer at pH 7.4 excited at 385 nm exhibits an emission maximum at 434 nm at room temperature. We measured the emission intensities of **1** in the presence of various concentrations of Zn^{2+} (0–1 mM; Figure 4). The emission intensity increased 19-fold upon addition of 2 equivalents of Zn^{2+}, and the emission maximum underwent a red shift (≈20 nm) to 454 nm. To understand this phenomenon further, metal-ion-selectivity assays were performed for **1** while keeping the other experimental conditions unchanged (Figure 5). Emission enhancement of **1** (50 μM) was not observed upon addition of 5 equivalents (2.5×10^{-4} M) of Na^+, K^+, Ca^{2+}, Mg^{2+}, or various d-block metal ions M (M = Mn^{2+}, Fe^{3+}, Cr^{3+}, Co^{2+}, Ni^{2+}, Cu^{2+}, Cd^{2+}) except for Cd^{2+}, which induced a

 © 2007 Wiley-VCH Verlag GmbH & Co. KGaA, Weinheim

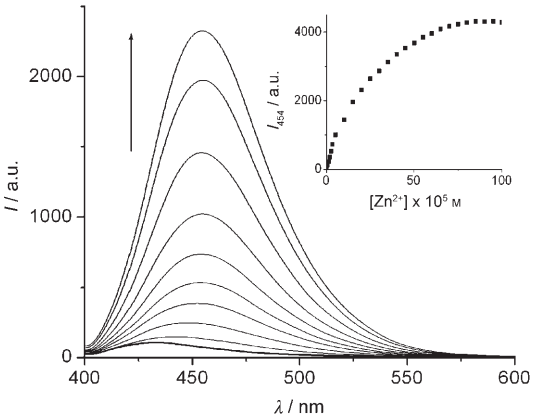

Figure 4. Luminescence emission spectra of 50 μM of complex **1** in the presence of 0, 7, 13, 20, 27, 33, 50, 100, 150, and 200 μM of free Zn^{2+} ions in 100 mM HEPES buffer at pH 7.4 at room temperature (excitation 385 nm, emission 454 nm). The inset shows the change in the luminescence intensity at $\lambda = 454$ nm as a function of the concentration of free Zn^{2+} in 100 mM HEPES buffer (pH 7.4).

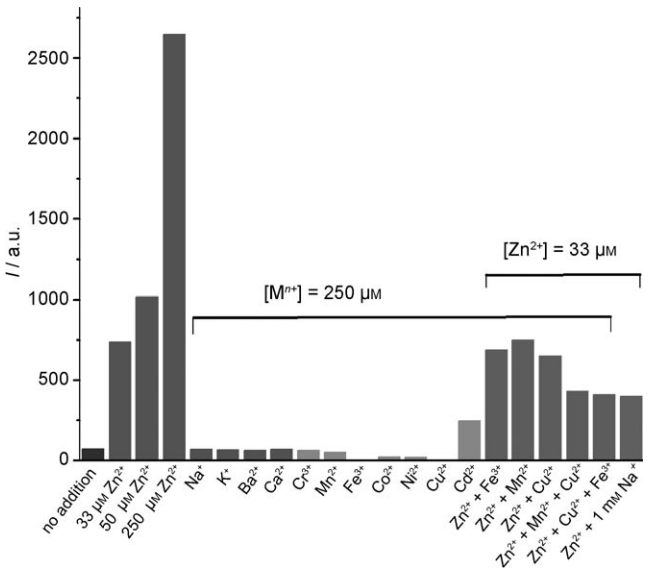

Figure 5. Luminescence emission intensity profile of **1** (50 μM) in the presence of various cations in 100 mM HEPES buffer at pH 7.4 at room temperature (excitation 385 nm, emission 454 nm).

slight enhancement of the emission intensity. However, Cd^{2+} is rarely present in biological systems, so this enhancement would not present a difficulty in biological applications. In the presence of a large excess (1 mM) of Na^+ together with Zn^{2+} (33.33 μM), almost no effect on the emission intensity of **1** was observed. Thus, Na^+, K^+, and so on, which exist at higher concentrations in biological systems, do not affect the luminescence intensity of **1**. The emission intensity was weakened or quenched upon the addition of several cations, for example, Fe^{3+}, Co^{2+}, Ni^{2+}, Cu^{2+}. In the presence of 5 equivalents of Cu^{2+}, Fe^{3+}, or Mn^{2+} together with Zn^{2+} (33.33 μM), no effect on the emission intensity of **1** was noted. Additionally, we measured the emission intensities of **1** in the presence of various counteranions of Zn^{2+}. There was no effect of counteranions (Cl^-, NO_3^-, CH_3COO^-, SO_4^{2-}, and ClO_4^-) on the intensities (see Supporting Information, Figure S1). Thus, Zn^{2+} can be distinguished from these metal ions.

A question hangs over the exact nature of the complex species involved in Zn^{2+} binding. The diffused reflection spectrum of **1** at 645 nm differs from its electronic spectrum in HEPES buffer (pH 7.4) and shows a blue shift of about 35 nm (Figure 6). This is quite significant and indicates the

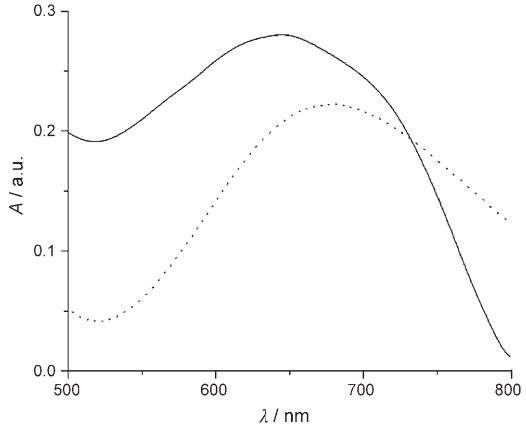

Figure 6. Absorption spectra of **1** in the solid state (——) and in 100 mM HEPES buffer (pH 7.4) (-----).

modification of the coordination sphere of the metal ion in solution. In water, the ESI mass spectrum shows peaks at $m/z = 911$ and 643 that can be assigned to $[Cu_2(HL)_2(H_3L)]\cdot 2H_2O$ (**2**) and $[Cu_2(HL)_2]\cdot H_2O$, respectively (Figure 7). The isotopic distributions for the above molecular species in water obtained experimentally correspond to the simulated patterns. Notably, the species do not contain any azide ions. No indication of the presence of the N_3^- moiety was obtained from FTIR spectra in solution. This may be due to the formation of the azide salt of copper ion, which was precipitated during the preparation of the solution. The IR spectrum of the freshly precipitated mass indicates the presence of azide ion at 2105 cm^{-1}. Equation (1) shows the dissociation of **1** into **2** in aqueous solution.

$$\{[Cu_2(HL)(N_3)]\cdot ClO_4\}_\infty\ (\mathbf{1}) \xrightarrow{H_2O} [Cu_2(HL)_2(H_3L)]\cdot 2H_2O\ (\mathbf{2}) + N_3^- + ClO_4^- + \tfrac{4}{3}Cu^{2+} + \tfrac{2}{3}OH^- \quad (1)$$

The increase in emission in the presence of Zn^{2+} is accounted for by the Zn^{2+} coordination of **2** in the unused binding site (Scheme 1). The ESI mass spectrum of the Zn^{2+}-coordinated complex of **2** reveals the formation of $[Cu_2Zn_2(HL)_3(Cl)_2]$ (Figure 8). A Job plot analysis reveals that the maximum emission is obtained at a **2**/Zn^{2+} ratio of 1:2. These data suggest that **2** in solution should form a 1:2

 © 2007 Wiley-VCH Verlag GmbH & Co. KGaA, Weinheim

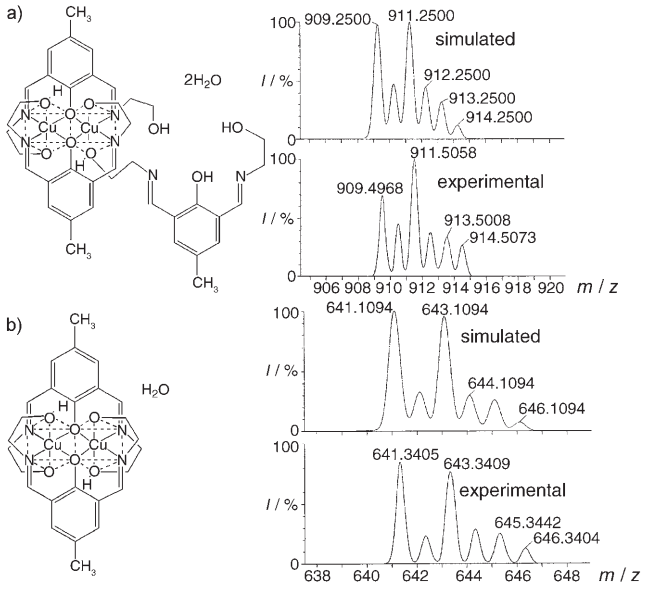

Figure 7. ESI mass spectra of **1** in water showing peaks at a) $m/z = 911$ and b) $m/z = 643$, which can be assigned to $[M+H]^+$ and $[M-(H_3L+H_2O)+H]^+$, respectively ($M = [Cu_2(HL)_2(H_3L)]\cdot 2H_2O$).

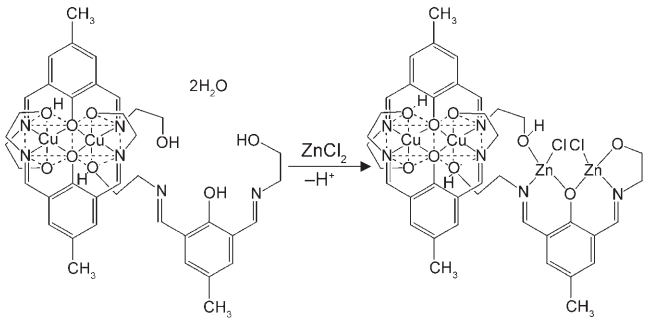

Scheme 1. Zn^{2+} coordination of **2** at the unused binding site.

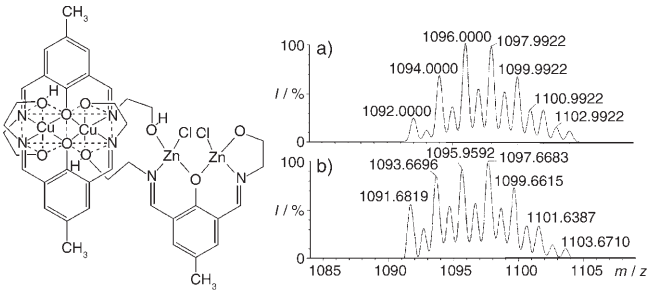

Figure 8. ESI mass spectra of the Zn^{2+}-cordinated complex of **2** in water showing the peak at $m/z = 1097$, which can be assigned to $[M+Na]^+$ ($M = [Cu_2Zn_2(HL)_3(Cl)_2]$). a) Simulated spectrum; b) experimental spectrum.

complex with Zn^{2+}. Unfortunately, we were unable to isolate the Zn^{2+}-bound complex of **2**. Further attempts to ascertain that complex **2** is responsible for Zn^{2+} binding were made by obtaining a further ESI mass spectrum with the addition of Cd^{2+} in place of Zn^{2+}, as Cd^{2+} induces a slight enhancement of the emission intensity. In water, the mass spectrum shows a peak at $m/z = 648$ that can be assigned to $\{[Cu_2Cd_2(HL)_2(H_2L)(Cl)(H_2O)_4]\cdot 5H_2O\}^{2+}$. The isotopic distributions for the above molecular species obtained experimentally (see Supporting Information, Figure S2) correspond to the simulated patterns. We also examined the effect of Zn^{2+} addition on the emission spectrum of the ligand (H_3L) itself. Zn^{2+} does not change the emission intensity of the ligand (Figures 9 and S3). This means that the

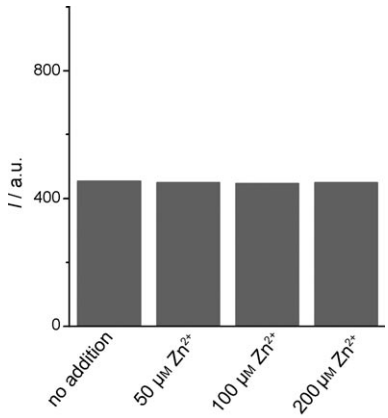

Figure 9. Emission intensity change profile of H_3L (50 μM) in the presence of various concentrations of Zn^{2+} in 100 mM HEPES buffer at pH 7.4 at room temperature (excitation 440 nm, emission 530 nm).

photoinduced electron transfer (PET) operating between the ligand receptor (R) (here O, N atoms of H_3L) and the fluorophore (F) is not perturbed during Zn^{2+} binding with the receptor. But, in case of Zn^{2+} binding with **2**, receptor sites can be simultaneously attached with different metal ions, in which case the PET of **2** is retarded. Thus, the enhancement of fluorescence is attributed to the disruption of PET communication between the receptor and the fluorophore moiety.[24] Another possibility is that the coordination of Zn^{2+} would impose rigidity and, hence, decrease the nonradiative decay of the excited state. The coordination of **2** to Zn^{2+} caused a 20-nm Stokes shift of the emission band and an approximately 15-fold increase in fluorescence quantum yield (Φ_f) (Table 3). The Stokes shift of the fluorescence

Table 3. Radiative and total nonradiative rate data.

Compound	τ_f [ns]	Φ_f	k_r [10^6 s^{-1}]	k_{nr} [10^8 s^{-1}]	χ^2
1	3.1	0.0106	3.38	3.15	1.136
1+Zn^{2+} (1:1)	3.7	0.1184	31.49	2.34	1.222
1+Zn^{2+} (1:2)	3.9	0.1685	43.68	2.15	1.262

maximum of **1** is due to an enhanced separation of charge in the electron-donor–acceptor fluorophore **1** on complexation. It is known that the late first-row transition-metal ions have a preference for complexation with N and O donor ligands. However, in the present case, effective binding occurs only with Zn^{2+}, which is reminiscent of the Job plot analysis. To

 © 2007 Wiley-VCH Verlag GmbH & Co. KGaA, Weinheim

examine the extent of binding interaction with Zn^{2+} in buffer, the binding constant was determined from the emission-intensity data by the modified Benesi–Hildebrand equation [Eq. (2)]:[25]

$$1/\Delta F = 1/\Delta F_{max} + (1/KC)(1/\Delta F_{max}) \quad (2)$$

in which $\Delta F = F_x - F_0$ and $\Delta F_{max} = F_\infty - F_0$, F_0, F_x, and F_∞ are the emission intensities of **1** in the absence of Zn^{2+}, at an intermediate Zn^{2+} concentration, and at a concentration of complete interaction, respectively, K is the binding constant, and C is the Zn^{2+} concentration (Figure 10). The binding

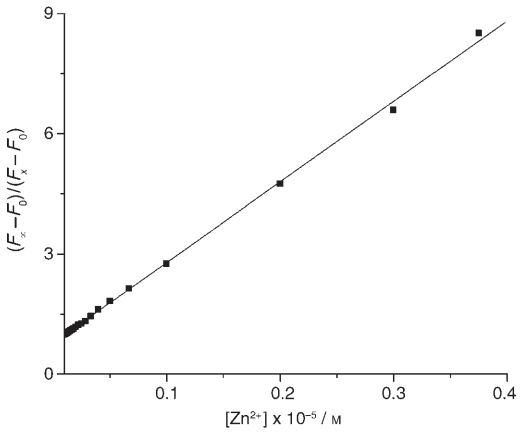

Figure 10. Determination of the binding constant K (±15%) of Zn^{2+} with **2** from the slope of the plot of Equation (2) as described in the text.

constant, K (±15%), was evaluated to be $5.0 \times 10^4\,M^{-1}$. We also studied the effect of Zn^{2+} addition on the fluorescence decay of **1**. The fluorescence lifetime (τ) of **1** in working buffer was 3.1 ns. In the presence of various concentrations of Zn^{2+}, longer fluorescence lifetimes were detected, thus confirming the inhibition of PET upon Zn^{2+} binding (Figure 11). The radiative rate constant k_r and total nonradiative rate constant k_{nr} of **1** as well as **1** bound to Zn^{2+} were calculated according to Equation (3)[26] and listed in Table 3. The data suggest that k_{nr} was only slightly changed, and the factor that induces fluorescence enhancement is mainly ascribed to the increase in k_r.

$$\tau^{-1} = k_r + k_{nr},\ k_r = \Phi_f/\tau \quad (3)$$

pH-Dependent Behavior

Besides metal-ion selectivity, it is important for many biological applications that the sensor does not respond to changes in pH.[23b] We measured the emission intensity of **1** at various pH values (Figure 12) in the presence and absence of Zn^{2+} with excitation at 385 nm. There was almost no effect of H^+ on the emission spectrum of **1** between pH 5.5 and 9 either in the presence or the absence of Zn^{2+}.

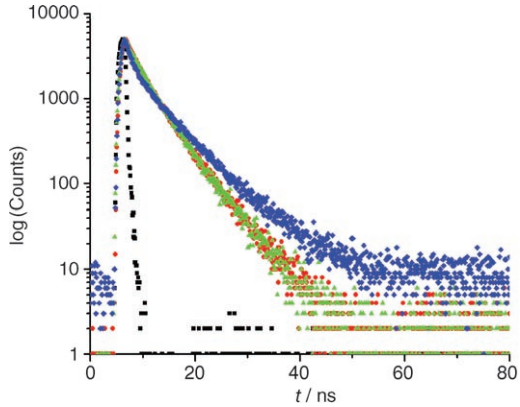

Figure 11. Time-resolved fluorescence decay of **1** in the absence and presence of different mole ratios of added Zn^{2+} in 100 mM HEPES buffer at pH 7.4 at room temperature (λ_{ex} = 370 nm). ■ = Lamp profile, ◆ = **1**, ● = **1** + Zn^{2+} (1:1), ▲ = **1** + Zn^{2+} (1:2).

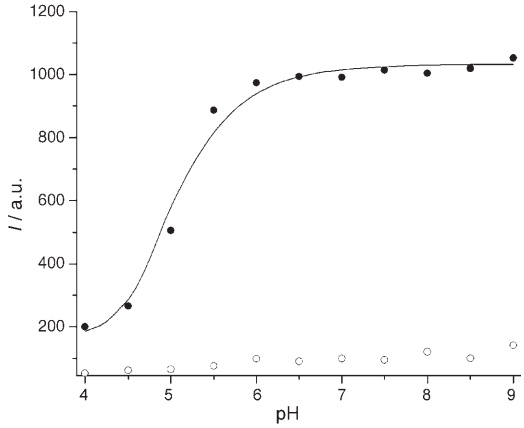

Figure 12. Effect of pH on the emission intensity of **1** in the absence (○) and presence of Zn^{2+} (●). 100 μM of Zn^{2+} was added to 50 μM of **1**.

Thus, the luminescence emission intensity of **1** is stable at physiological pH.

Biological Applications of 1

We examined the application of **1** to cultured living cells (B16F10 mouse melanoma and A375 human melanoma) by fluorescence microscopy (B16F10: Figure 13; A375: Figure 14). As **1** can be excited by light of a relatively long wavelength, this compound is suitable for cellular applications, in contrast to the previously reported Zn^{2+}-selective luminescent sensors.[23c] After incubation with 10 μM of **1** in PBS (phosphate-buffered saline), the cells displayed modest intracellular staining, which suggests that **1** can be used intracellularly.[23b] Next, we examined whether the difference in affinity is related by fluorescence microscopic imaging of intracellular Zn^{2+}. The intracellular concentration of Zn^{2+} was controlled with a Zn^{2+} ionophore, pyrithione (2-mercaptopyridine *N*-oxide), which brings extracellular Zn^{2+} into the cytoplasm. We added various concentrations of Zn^{2+} to

 © 2007 Wiley-VCH Verlag GmbH & Co. KGaA, Weinheim

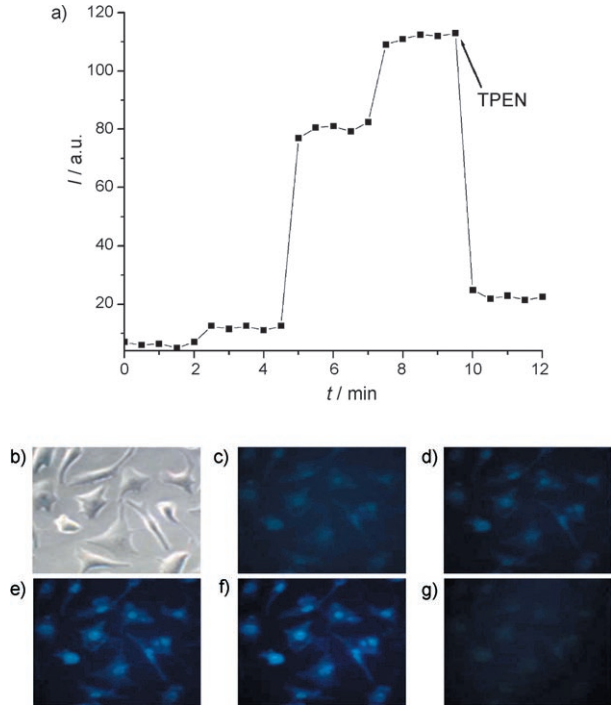

Figure 13. Phase-contrast and fluorescence response of **1** induced by intracellular Zn^{2+}. a) B16F10 cells incubated with 10 μM of **1** for 60 min at room temperature were washed with PBS, and fluorescence excitation at 330–385 nm was measured at 30-s intervals. Cells were exposed to pyrithione (100 μM) in the presence of increasing concentrations of added extracellular Zn^{2+}, as indicated by the solid line. Return of intracellular Zn^{2+} to the rest level was achieved by addition of TPEN (200 μM, indicated by arrow). b) Phase-contrast image taken at 0 min. c–g) Fluorescence images of the cells incubated with **1** (c: 2 min), with pyrithione and 50 μM Zn^{2+} (d: 4 min), with 100 μM Zn^{2+} (e: 7 min), with 150 μM Zn^{2+} (e: 7 min), with 150 μM Zn^{2+} (f: 9 min), and with 200 μM TPEN (g: 11 min).

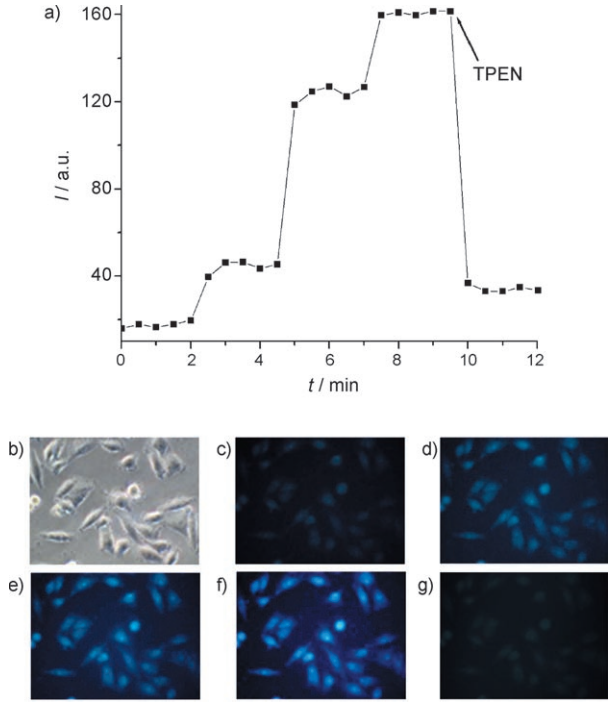

Figure 14. Phase-contrast and fluorescence response of **1** induced by intracellular Zn^{2+}. a) A375 cells incubated with 10 μM of **1** for 60 min at room temperature were washed with PBS, and fluorescence excitation at 330–385 nm was measured at 30-s intervals. Cells were exposed to pyrithione (100 μM) in the presence of increasing concentrations of added extracellular Zn^{2+}, as indicated by the solid line. Return of intracellular Zn^{2+} to the rest level was achieved by addition of TPEN (200 μM, indicated by arrow). b) Phase-contrast image taken at 0 min. c–g) Fluorescence images of the cells incubated with **1** (c: 2 min), with pyrithione and 50 μM Zn^{2+} (d: 4 min), with 100 μM Zn^{2+} (e: 7 min), with 150 μM Zn^{2+} (f: 9 min), and with 200 μM TPEN (g: 12 min).

pyrithione, and the intracellular Zn^{2+} concentration was measured by fluorescence microscopy. When the extracellular Zn^{2+} concentration was increased from 50 to 150 μM, the saturation of fluorescence intensity of **1** was not achieved until 150 μM of Zn^{2+}. The fluorescence was measured at 30-s intervals for various concentrations of $ZnCl_2$ (Figures 13a and 14a). The cells became noticeably more fluorescent when 150 μM $ZnCl_2$ and 100 μM pyrithione were added, which facilitated Zn^{2+} diffusion into the cells. The different response of **1** with various concentrations of added Zn^{2+} is clearly evident from Figures 13 and 14. Subsequent addition of the cell-permeable metal chelator *N*,*N*,*N*′,*N*′-tetrakis(2-pyridylmethyl)ethylenediamine (TPEN) quenched the emission, which is consistent with intracellular turn-on as a consequence of reversible zinc binding.[23b,c] These results suggest that **1** can be used to monitor the changes of intracellular Zn^{2+}, and should, therefore, be useful for clarifying the role of Zn^{2+} in biological processes in which the intracellular concentration of Zn^{2+} is important, for example, in cell death induced by ischemia.[27] However, it is important to mention here that measurement of cell viability forms the basis for numerous in vitro assays of the response of a cell population to external factors. Thus, for biological application, **1** should not be cytotoxic at its applied dose and time of incubation. To test its cytotoxicity, we performed an MTT (3-(4,5-dimethylthiazol-2-yl)-2,5-diphenyltetrazolium bromide) assay with both B16F10 and A375 cells treated with 10 μM of **1** for up to 12 h. The MTT assay, first described by Mosmann,[28] is based on the ability of the mitochondrial dehydrogenase enzyme from viable cells to cleave the tetrazolium rings of yellow MTT and form dark-blue formazan crystals that are largely impermeable to cell membranes, thus resulting in its accumulation within metabolically active or so-called viable cells. The number of surviving viable cells is thus directly proportional to the level of the formazan product created. The resulting intracellular formazan can then be solubilized and quantified by spectrophotometric means. The MTT assay thus measures cell proliferation rate and, conversely, when metabolic events lead to cell death because of cytotoxicity, reduction in cell viability. As shown in Figure S4 of the Supporting Information, 10 μM of **1** did not show significant cytotoxic effects on both B16F10 and A375 cells up to 6 h of its treatment, although there was significant cytotoxicity from 6 h onwards. This therefore sug-

 © 2007 Wiley-VCH Verlag GmbH & Co. KGaA, Weinheim

gests that **1** can be readily used for cellular application at the indicated dose and time of incubation without concern about its cytotoxicity.

Besides cultured living-cell systems, we applied **1** to rat hippocampal slices. The slices were incubated with 10 μM of **1** for 1 h in ACSF (artificial cerebrospinal fluid) at room temperature. The fluorescence was dense mainly in three regions: the dentate gyrus (DG), CA3, and CA1 (CA = cornu ammonis), which were indistinguishable (Figure 15). Therefore, no regional difference in released Zn^{2+} concentration was observed, probably because of high affinity for Zn^{2+}. This distribution was also detected by other staining methods.[23b] The fluorescence was quenched by incubation of the slices with 200 μM TPEN for 0.5 h. Thus, **1** can be used to detect intracellular free Zn^{2+} in hippocampal slices.

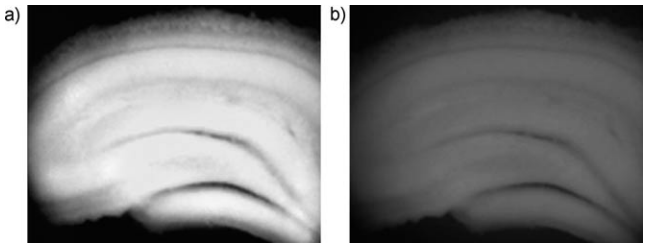

Figure 15. Fluorescence images of **1**-loaded rat hippocampal slices. The slices were incubated with 10 μM of **1** for 1 h at room temperature in ACSF and then washed with ACSF for 30 min. Fluorescence microscopy images a) before and b) after incubation with 200 μM TPEN for 0.5 h at room temperature.

Conclusions

We have synthesized a luminescent 2D coordination compound based on a 3d-metal ion, $\{[Cu_2(HL)(N_3)]\cdot ClO_4\}_\infty$ (**1**), which displayed high selectivity for Zn^{2+} and can be used as a zinc ion selective luminescent probe for biological application. Complex **1** dissociates in solution to produce $[Cu_2(HL)_2(H_3L)]\cdot 2H_2O$ (**2**), which acts as a metalloligand. The increase in emission in the presence of Zn^{2+} is accounted for by Zn^{2+} coordination of **2** at the unused binding site to form $[Cu_2Zn_2(HL)_3(Cl)_2]$. An approximately 19-fold Zn^{2+}-selective chelation-enhanced fluorescence response in HEPES buffer (pH 7.4) was attributed possibly to the disruption of PET communication between the receptor and fluorophore moieties or by structural rigidity through coordination with Zn^{2+}. By incubating cultured living cells or rat hippocampal slices with **2**, intracellular and free Zn^{2+} concentrations in hippocampal slices could be monitored. These results provide an opening into the promising new field of luminescent probes with 3d-metal-based coordination compounds for studies on the biological functions of Zn^{2+}.

Experimental Section

Materials and Physical Methods

All reagents and chemicals were purchased from Sigma and used without further purification. PBS buffer was prepared by using deionized and sonicated triply distilled water. Solvents used for spectroscopic studies were purified and dried by standard procedures before use. FTIR spectra were obtained on a Nicolet MAGNA-IR 750 spectrometer with samples prepared as KBr pellets. Elemental analysis was carried out on a 2400 Series-II CHN analyzer (Perkin–Elmer, USA). Luminescence spectra were obtained on a Hitachi 4500 luminescence spectrometer. Fluorescence lifetimes were determined from time-resolved intensity decay with the method of time-correlated single-photon counting by using a picosecond diode laser at 370 nm as the light source. ESI mass spectra were recorded on a Qtof Micro YA263 mass spectrometer.

Caution: Perchlorate salts of metal complexes with organic ligands are potentially explosive. Only a small amount of material should be prepared and handled with caution.

Syntheses

H_3L: The ligand 2,6-bis(hydroxyethyliminoethyl)-4-methyl phenol was synthesized by following the published procedure.[29]

1: A methanolic solution (20 mL) of $Cu(ClO_4)_2\cdot 6H_2O$ (0.30 g, 0.81 mmol) was added slowly to a magnetically stirred methanolic solution (15 mL) of H_3L (0.09 g, 0.36 mmol). The mixture was stirred in air for 45 min while NEt_3 (0.10 mL, 0.72 mmol) was added, whereby a deep-green solution was formed. An aqueous solution (10 mL) of NaN_3 (0.023 g, 0.36 mmol) was added, and the mixture was heated at reflux for 1 h. The solution was then cooled to ambient temperature, filtered, and kept under air. Single crystals of **1** (0.63 g, 75 %) for X-ray crystallography were obtained upon slow evaporation of the filtrate at ambient temperature for a few days. FTIR (KBr): 3361 (br), 2100 (vs), 1654 (vs), 1629 (vs), 1560 (vs), 1448 (m), 1330 (m), 1240 (w), 1117 (vs), 623 cm^{-1} (s) (br = broad, w = weak, m = medium, s = strong, vs = very strong); elemental analysis: calcd (%) for $C_{13}H_{16}N_5O_7ClCu_2$: C 30.21, H 3.12, N 13.54; found: C 30.10, H 3.09, N 13.42.

X-ray Data Collection and Structure Determination

Crystal data are summarized in Table 1. The diffraction experiment was carried out on a Bruker SMART CCD area-detector diffractometer at 150 K. No crystal decay was observed, so no time-decay correction was needed. The collected frames were processed with the software SAINT,[30] and an empirical absorption correction was applied (SADABS)[31] to the collected reflections. The calculations were performed by using the Personal Structure Determination Package[32] and the physical constants tabulated therein.[33] The structure was solved by direct methods (SHELXS)[34] and refined by full-matrix least squares with all reflections and by minimizing the function $\Sigma w(F_o^2 - kF_c^2)^2$ (refinement on F^2). All non-hydrogen atoms were refined with anisotropic thermal factors. Hydrogen atoms H1–H4 were refined with a fixed isotropic thermal parameter. All the other hydrogen atoms were placed in their ideal positions (C–H = 0.97 Å), with the thermal parameter B at 1.10 times that of the carbon atom to which they are attached, and were not refined. In the final Fourier map, the maximum residual was 1.45(28) e $Å^{-3}$ at 1.10 Å from N1.

CCDC-626266 contains the supplementary crystallographic data for this paper. These data can be obtained free of charge from the Cambridge Crystallographic Data Centre at www.ccdc.cam.ac.uk/data_request/cif.

Fluorimetric Analysis

Fluorescence spectroscopic studies were performed with a Hitachi 4500 luminescence spectrometer. The slit width was 2.5 nm for both excitation and emission. The photomultiplier voltage was 700 V. Emission quantum yields (Φ) were estimated by integrating the area under the fluorescence curves with the formula [Eq. (4)]:

$$\Phi_{sample} = \frac{OD_{standard} \times A_{sample}}{OD_{sample} \times A_{standard}} \times \Phi_{standard} \quad (4)$$

 © 2007 Wiley-VCH Verlag GmbH & Co. KGaA, Weinheim

in which A is the area under the emission spectral curve and OD is optical density of the compound at the excitation wavelength.[35] The standard used for the measurement of fluorescence quantum yield was coumarin 343 ($\Phi = 0.63$ in ethanol).[36]

Imaging System

The imaging system comprised an inverted fluorescence microscope (IX-70, Olympus, Tokyo, Japan), a digital compact camera (Olympus, model C-5060), and an image processor (Camedia Master, Olympus, Japan). The microscope was equipped with a halogen lamp, a mercury burner, an objective lens (×40 (B16F10 and A375) or ×5 (hippocampal slice), and an excitation filter (330–385 nm).

Preparation of Cells

A375 human melanoma and B16F10 mouse melanoma cells procured from the National Center for Cell Science, Pune, India were cultured in Dulbecco's modified Eagle's medium (DMEM; Gibco BRL) supplemented with fetal bovine serum (FBS; 10%, Gibco BRL) and an antibiotic mixture (1%) containing penicillin, streptomycin, and neomycin (PSN; Gibco BRL) at 37°C in a humidified incubator with CO_2 (5%). For experimental study, cells were grown to 80–90% confluence, harvested with trypsin (0.025%, Gibco BRL) and EDTA (0.52 mM, Gibco BRL) in PBS (Sigma Diagnostics), and plated in a six-well culture plate (NUNC, Roskilde, Germany) at a density of 5×10^5 cells per mL. The cells were then rinsed with PBS, incubated with PBS containing **1** (10 μM) for 1 h at 37°C, washed with PBS thrice, and mounted on a microscope stage.

To test the cytotoxicity of **1**, an MTT assay was performed by the procedure described earlier.[37] Briefly, cells (1×10^5 per well) grown in a 96-well culture plate (NUNC, Roskilde, Denmark) for 24 h were treated with DMEM supplemented with FBS (10%) and PSN (1%), both with and without **1** (10 μM), for different time intervals. Thereafter, the cells were incubated with a medium containing MTT (0.5 mg mL^{-1}) for a further 4 h. The intracellular formazan crystals formed were solubilized with acidic isopropanol (0.04 N), and the absorbance of the solution was measured at 595 nm by using an ELISA reader (Model: Emax, Molecular Device, USA).

Preparation of Rat Hippocampal Slices

The whole brains of Adult male Sprague-Dawley rats (body weight 200–250 g) were removed quickly under diethyl ether anesthesia and placed in ice-cold ACSF, which was aerated with O_2 (95%)/CO_2 (5%). The composition of the ACSF was NaCl (124 mM), KCl (2.5 mM), $NaHCO_3$ (26 mM), NaH_2PO_4 (1.25 mM), $CaCl_2$ (2.0 mM), $MgCl_2$ (1.0 mM), and glucose (10 mM). The hippocampus was isolated, placed on an agar plate, and sliced into 300-μm-thick slices with an oscillating microtome (Electron Microscopy Sciences, Model OTS-4000). The fresh hippocampal slices were incubated in ACSF equilibrated with O_2 (95%)/CO_2 (5%) for more than 45 min at room temperature, then they were loaded with **1** (10 μM) for 1 h at room temperature. Postincubation with ACSF was carried out for 30 min to wash out the extracellular compound (**1**). A small flow-through chamber, whose base consisted of a thin glass cover slip, was placed on a microscope stage. A loaded slice was then held in place in the chamber by a metal wire ring with a stretched nylon net and continuously perfused (2.5 mL min^{-1}) with equilibrated ACSF at 33–34°C.

Effect of pH on Luminescence Intensity

The following buffers were used: AcOH/AcONa buffer (100 mM, pH 4.0–5.5), morpholinoethanesulfonic acid (MES) buffer (100 mM, pH 5.5–6.5), HEPES buffer (100 mM, pH 7.0–8.0), and *N*-cyclohexyl-2-aminoethanesulfonic acid (CHES) buffer (100 mM, pH 8.5–9.0).

Measurements of Metal-Ion Selectivity

Metal ions were added as $MnCl_2$, $FeCl_3$, $CrCl_3$, $CoCl_2$, $NiCl_2$, $CuCl_2$, $ZnCl_2$, $CdCl_2$, NaCl, KCl, $CaCl_2$, and $MgCl_2$. The emission of **1** was measured in HEPES buffer (100 mM, pH 7.4) at room temperature (excitation 385 nm, emission 454 nm).

Acknowledgements

K.D. acknowledges the Council of Scientific and Industrial Research, New Delhi, India, for financial support. We appreciate the cooperation received from Prof. Nitin Chattopadhyay and Dr. Arabinda Mallick of the Department of Chemistry, Jadavpur University. Thanks are due to all the referees for their helpful criticism.

[1] a) A. Takeda, *BioMetals* **2001**, *14*, 343–351; b) B. L. Vallee, K. S. Falchuk, *Physiol. Rev.* **1993**, *73*, 79–118.
[2] a) T. Valente, C. Auladell, *Mol. Cell. Neurosci.* **2002**, *21*, 189–204; b) T. B. Cole, H. J. Wenzel, K. E. Kafer, P. A. Schwartzkroin, R. D. Palmiter, *Proc. Natl. Acad. Sci. USA* **1999**, *96*, 1716–1721.
[3] a) M. Vasak, D. W. Hasler, *Curr. Opin. Chem. Biol.* **2000**, *4*, 177–183; b) C. Jacob, W. Maret, B. L. Vallee, *Proc. Natl. Acad. Sci. USA* **1998**, *95*, 3489–3494; c) M. Ebadi, P. L. Iversen, R. Hao, D. R. Cerutis, P. Rojas, H. K. Happe, L. C. Murrin, R. F. Pfeiffer, *Neurochem. Int.* **1995**, *27*, 1–22.
[4] a) T. Budde, A. Minta, J. A. White, A. R. Kay, *Neuroscience* **1997**, *79*, 347–358; b) C. J. Frederickson, D. W. Moncrieff, *Biol. Signals* **1994**, *3*, 127–139; c) C. J. Frederickson, *Int. Rev. Neurobiol.* **1989**, *31*, 145–238; d) Y. V. Li, C. J. Hough, J. M. Sarvey, *Sci. STKE* **2003**, pe19.
[5] a) D. G. Themelis, P. D. Tzanavaras, A. A. Liakou, H. D. Tzanavaras, J. K. Papadimitriou, *Analyst* **2000**, *125*, 2106–2111; b) M. M. Paker, F. L. Humaller, D. J. Mahler, *Clin. Chem.* **1967**, *13*, 40–48.
[6] J. M. Berg, Y. Shi, *Science* **1996**, *271*, 1081–1085.
[7] P. D. Zalewski, S. H. Millard, I. J. Forbes, O. Kapaniris, A. Slavotinek, W. H. Betts, A. D. Ward, S. F. Lincoln, I. Mahadevan, *J. Histochem. Cytochem.* **1994**, *42*, 877–884.
[8] P. D. Zalewski, X. Zian, L. L. L. Soon, W. G. Breed, R. F. Seamark, S. F. Lincoln, A. D. Ward, F. Z. Sun, *Reprod. Fertil. Dev.* **1996**, *8*, 1097–1105.
[9] A. Q. Truong-Tran, L. H. Ho, F. Chai, P. D. Zalewski, *J. Nutr.* **2000**, *130*, 1459S–1466S.
[10] D. W. Choi, J. Y. Koh, *Annu. Rev. Neurosci.* **1998**, *21*, 347–375.
[11] C. J. Frederickson, M. D. Hernandez, J. F. McGinty, *Brain Res.* **1989**, *480*, 317–321.
[12] A. I. Bush, W. H. Pettingell, G. Multhaup, M. D. Paradis, J. P. Vonsattel, J. F. Gusella, K. Beyreuther, C. L. Masters, R. E. Tanzi, *Science* **1994**, *265*, 1464–1467.
[13] a) A. R. Kay, *J. Neurosci.* **2003**, *23*, 6847–6855; b) T. B. Cole, A. Martyanova, R. D. Palmiter, *Brain Res.* **2001**, *891*, 253–265.
[14] a) S. C. Burdette, S. J. Lippard, *Proc. Natl. Acad. Sci. USA* **2003**, *100*, 3605–3610; b) S. C. Burdette, S. J. Lippard, *Coord. Chem. Rev.* **2001**, *216–217*, 333–361.
[15] E. Kimura, T. Koike, *Chem. Soc. Rev.* **1998**, *27*, 179–184.
[16] a) C. J. Chang, S. J. Lippard, *Met. Ions Life Sci.* **2006**, *1*, 321–370; b) P. Jiang, Z. Guo, *Coord. Chem. Rev.* **2004**, *248*, 205–229; c) E. Kimura, S. Aoki, *Biometals* **2001**, *14*, 191–204.
[17] C. J. Frederickson, E. J. Kasarskis, D. Ringo, R. E. Frederickson, *J. Neurosci. Methods* **1987**, *20*, 91–103.
[18] P. D. Zalewski, I. J. Forbes, W. H. Betts, *Biochem. J.* **1993**, *296*, 403–408.
[19] M. Taki, J. L. Wolford, T. V. O'Halloran, *J. Am. Chem. Soc.* **2004**, *126*, 712–713.
[20] a) C. J. Chang, E. M. Nolan, J. Jaworski, S. C. Burdette, M. Sheng, S. J. Lippard, *Chem. Biol.* **2004**, *11*, 203–210; b) C. J. Chang, E. M. Nolan, J. Jaworski, K.-I. Okamoto, Y. Hayashi, M. Sheng, S. J. Lippard, *Inorg. Chem.* **2004**, *43*, 6774–6779; c) S. C. Burdette, C. J. Frederickson, W. Bu, S. J. Lippard, *J. Am. Chem. Soc.* **2003**, *125*, 1778–1787; d) S. C. Burdette, G. K. Walkup, B. Spingler, R. Y. Tsien, S. J. Lippard, *J. Am. Chem. Soc.* **2001**, *123*, 7831–7841; e) G. K. Walkup, S. C. Burdette, S. J. Lippard, *J. Am. Chem. Soc.* **2000**, *122*, 5644–5645.
[21] a) T. Hirano, K. Kikuchi, Y. Urano, T. Nagano, *J. Am. Chem. Soc.* **2002**, *124*, 6555–6562; b) T. Hirano, K. Kikuchi, Y. Urano, T. Higuchi, T. Nagano, *J. Am. Chem. Soc.* **2000**, *122*, 12399–12400.

 © 2007 Wiley-VCH Verlag GmbH & Co. KGaA, Weinheim

[22] a) A. M. D. Shults, D. A. Pearce, B. Imperiali, *J. Am. Chem. Soc.* **2003**, *125*, 10591–10597; b) H. A. Godwin, J. M. Berg, *J. Am. Chem. Soc.* **1996**, *118*, 6514–6515.
[23] a) C. R. Goldsmith, S. J. Lippard. *Inorg. Chem.* **2006**, *45*, 555–561; b) K. Komatsu, K. Kikuchi, H. Kojima, Y. Urano, T. Nagano, *J. Am. Chem. Soc.* **2005**, *127*, 10197–10204; c) K. Hanaoka, K. Kikuchi, H. Kojima, Y. Urano, T. Nagano, *J. Am. Chem. Soc.* **2004**, *126*, 12470–12476; d) B. Zhao, X.-Y. Chen, P. Cheng, D.-Z. Liao, S.-P. Yan, Z.-H. Jiang, *J. Am. Chem. Soc.* **2004**, *126*, 15394–15395; e) C. C. Woodroofe, S. J. Lippard, *J. Am. Chem. Soc.* **2003**, *125*, 11458–11459.
[24] M. Sarkar, S. Banthia, A. Samanta, *Tetrahedron Lett.* **2006**, *47*, 7575–7578.
[25] a) A. Mallick, N. Chattopadhyay, *Photochem. Photobiol.* **2005**, *81*, 419–424; b) H. A. Benesi, J. H. Hildebrand, *J. Am. Chem. Soc.* **1949**, *71*, 2703–2707.
[26] N. J. Turro, *Modern Molecular Photochemistry*, Benjamin Cummings Publishing Company, Inc., Menlo Park, **1978**.
[27] J.-Y. Koh, S. W. Suh, B. J. Gwag, Y. Y. He, C. Y. Hsu, D. W. Choi, *Science* **1996**, *272*, 1013–1016.
[28] T. Mosmann, *J. Immunol. Methods* **1983**, *65*, 55–63.
[29] W.-X. Zhang, C.-Q. Ma, X.-N. Wang, Z.-G. Yu, Q.-J. Lin, D.-H. Jiang, *Chin. J. Chem.* **1995**, *13*, 497–503.
[30] SAINT Reference Manual, Siemens Energy and Automation, Madison, WI (USA), **1994–1996**.
[31] G. M. Sheldrick, SADABS, Empirical Absorption Correction Program, University of Göttingen, Göttingen (Germany), **1997**.
[32] B. A. Frenz, *Comput. Phys.* **1988**, *2*, 42.
[33] *Crystallographic Computing 5*, Oxford University Press, Oxford, **1991**, chap. 11, p. 126.
[34] G. M. Sheldrick, SHELXS-86, Program for the Solution of Crystal Structures, University of Gottingen, Göttingen (Germany), **1985**.
[35] E. Austin, M. Gouterman, *Bioinorg. Chem.* **1978**, *9*, 281–298.
[36] G. A. Reynolds, K. H. Drexhage, *Opt. Commun.* **1975**, *13*, 222–225.
[37] J. Ratha, K. A. Majumdar, S. K. Mandal, R. Bera, C. Sarkar, B. Saha, C. Mandal, K. D. Saha, R. Bhadra, *Mol. Cell. Biochem.* **2006**, *290*, 113–123.

Received: May 2, 2007
Published online: July 16, 2007

 © 2007 Wiley-VCH Verlag GmbH & Co. KGaA, Weinheim